Geophysical Research Letters

RESEARCH LETTER
10.1029/2018GL078855

Key Points:
- Ocean waves over small-scale topography produce both horizontal and vertical equivalent point forces
- Small-scale wavy bottoms are stronger sources of primary microseism than constant slopes
- The vertical force, caused by pressure modulations, is generally weaker than the horizontal force

Supporting Information:
- Supporting Information S1
- Figure S1
- Figure S2

Correspondence to:
F. Ardhuin,
ardhuin@ifremer.fr

Citation:
Ardhuin, F. (2018). Large-scale forces under surface gravity waves at a wavy bottom: A mechanism for the generation of primary microseisms. *Geophysical Research Letters*, *45*, 8173–8181. https://doi.org/10.1029/2018GL078855

Received 20 MAY 2018
Accepted 3 AUG 2018
Accepted article online 13 AUG 2018
Published online 20 AUG 2018

Large-Scale Forces Under Surface Gravity Waves at a Wavy Bottom: A Mechanism for the Generation of Primary Microseisms

Fabrice Ardhuin[1]

[1] University of Brest, CNRS, IRD, Ifremer, Laboratoire d'Océanographie Physique et Spatiale, IUEM, Brest, France

Abstract Primary microseisms are background seismic oscillations recorded everywhere on Earth with typical frequencies $0.05 < f < 0.1$ Hz. They appear to be generated by ocean waves of the same frequency f, propagating over shallow bottom topography. Previous quantitative models for the generation of primary microseisms considered wave propagation over topographic features with either large scales, equivalent to a vertical point force, or small scales matching ocean wave wavelengths, equivalent to a horizontal force. While the first requires unrealistic bottom slopes to explain measured Rayleigh wave amplitudes, the second produced Love waves and not enough Rayleigh waves. Here we show how the small scales actually produce comparable horizontal and vertical forces. For example, a realistic rough bottom over an area of 100 km^2 with depths around 15 m is enough to explain the vertical ground motion observed at a seismic station located 150 km away. Ocean waves propagating over small-scale topography is thus a plausible explanation for the observed microseisms at frequencies around 0.07 Hz.

Plain Language Summary Microseisms are background oscillations of the solid Earth. Most of these oscillations are caused by ocean waves and can thus be used to study their source, the ocean waves, or the medium in which they propagate, the solid Earth. Several theories have been proposed for how ocean waves going over shallow ocean topography make microseisms in the band of periods 10 to 20 s, but they are not satisfactory because they either require unrealistic large slopes of the ocean floor or they produce a ratio of different types of seismic waves, Love and Rayleigh waves, that is too large. We thus revise these theories to show that a plausible seismic source is the propagation ocean of waves over a *wavy bottom*, when the bottom has wavelengths that match those of ocean wave. We particularly verify that the predicted Rayleigh wave amplitude is of the order of what is measured at a particular seismometer located in Ireland. Because the necessary details in bottom topography vary a lot between different ocean regions, the new theory suggests that the spatial distribution of seismic sources is more heterogeneous than previously thought.

1. Introduction

A better quantitative understanding of seismic wave generation is important for solid Earth analyses, for example, using tomography (Retailleau et al., 2017; Shapiro et al., 2005), or for estimating ocean wave properties (e.g., Ardhuin et al., 2012). The mutual interaction of random ocean surface gravity waves or their interaction with random bottom topography can be treated by the general wave scattering theory of Hasselmann (1966, Figure 7). This theory predicts that the seismic energy at wavenumber vector $\mathbf{K}$ and frequency f grows linearly with propagation distance, if the resonance conditions $\mathbf{K} = \mathbf{k}_1 + \mathbf{k}_2$ and $f_s = f_1 + f_2$ are satisfied, where $(\mathbf{k}_1, f_1)$ and $(\mathbf{k}_2, f_2)$ are the wavenumber vectors and frequency of the interacting random wave fields.

This general theory includes the double-frequency mechanism by which pairs of wave trains with the same frequency $f = f_1 = f_2$ but opposing directions ($\mathbf{k}_1 \simeq -\mathbf{k}_2$) excite seismic waves at a frequency $f_s = 2f$ (Longuet-Higgins, 1950). The theory also includes a same-frequency mechanism, by which ocean waves with frequency $f = f_1$ propagating over a sloping seafloor, which is not moving and thus has a frequency $f_2 = 0$, generate seismic waves at the frequency $f_s = f$. This seismic generation is possible when an ocean wave wavenumber $\mathbf{k}$ nearly opposes a bottom wavenumber $\mathbf{k}_b$, so that the pattern of wave-induced pressure on the seafloor contains very large wavelengths with $\mathbf{K} = \mathbf{k} + \mathbf{k}_b$, including seismic wavelengths for the frequency

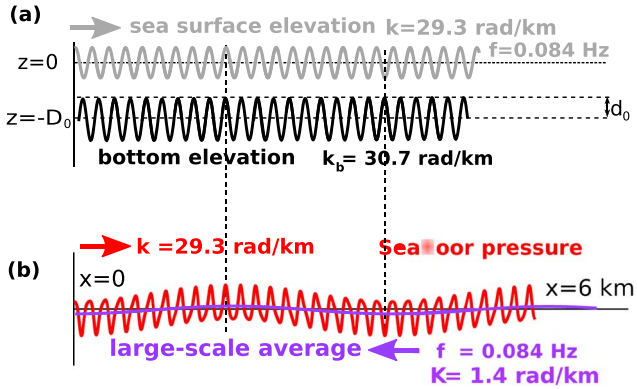

Figure 1. (a) Definition sketch of water depth and bottom elevation amplitude d. (b) Pressure at the seafloor in red. This pressure field contains long wavelength components (violet) that oscillate in time as given by equation (13) below, and in this example propagate from right to left at a speed of 3.7 km/s. This pattern is computed with $D_0 = 100$ m and $k_0 D_0 = 2.9$, which gives $\alpha < 0$. For animations see http://tinyurl.com/mswanim.

f_s. Before that generalization, Hasselmann (1963) considered a constantly sloping seafloor and computed the seismic response for frequencies 0.05 to 0.1 Hz, which is known as the primary microseism band. The seafloor pressure pattern is characterized by a power spectrum that is broad in the wavenumber domain and thus equivalent to a vertical point force from which the seismic response can be estimated (e.g., Gualtieri et al., 2013; Hasselmann, 1963).

That theory was applied successfully to slowly varying bottom slopes at seismic hum frequencies, lower than 0.03 Hz (Ardhuin et al., 2015). For primary microseisms with $0.05 < f < 0.1$ Hz, Hasselmann (1963) used a bottom slope of 3%. More recently, Ardhuin et al. (2015) showed that the primary microseismic signal measured at the French seismic station Saint Sauveur en Rue (Geoscope network) requires an average ocean bottom slope of 6% in water depths around 20 m, whereas average slopes on the French continental shelves are of the order of 0.1% or less. It is difficult to explain such a large difference with effects not included in these models such as three-dimensional seismic propagation or amplification by sediments.

Another reason why the constant or slowly varying bottom slope is not a satisfactory model for the primary microseisms is that the horizontal component of the equivalent point force, equal to the vertical force times the bottom slope, is too weak to explain the observed Love-wave kinetic energy (Friedrich et al., 1998; Juretzek & Hadziioannou, 2016; Nishida et al., 2008). The same constraint applies to the lower-frequency hum band. This is why Fukao et al. (2010) considered the effect of small-scale bottom topography in the form of isolated seamounts. These produce an equivalent shear force of reasonable order of magnitude for microseisms in the hum band at frequency under 0.03 Hz. That work was generalized by Saito (2010) who considered the horizontal force caused by surface waves over any topography described by a bottom elevation spectrum. However, Fukao et al. (2010) and Juretzek and Hadziioannou (2017) found that a combination of horizontal and vertical forces is required to arrive at the observed ratios of Love and Rayleigh waves.

Here we show that ocean waves propagating over small-scale bottom topography, as considered by Saito (2010), are equivalent to a combination of vertical and horizontal forces. We particularly focus on the previously overlooked vertical component. We also generalize the result of Saito (2010) to random ocean waves. The details of the bottom pressure and issues specific to the vertical force are described in section 2, first considering sinusoidal waves over a sinusoidal bottom, before generalizing to random waves over random bottom topography. Section 3 gives one example using a real ocean bottom topography, and conclusions follow in section 4.

2. Large-Scale Pressure Arising From Depth Modulations

We consider surface gravity waves propagating in the x direction. As illustrated in Figure 1, the bottom pressure at a wavy bottom with wavenumber k_b under ocean waves of wavenumber k and frequency f contains long components with wavenumber $K = k - k_b$, oscillating in time at frequency f. As k approaches k_b, the horizontal propagation speed of these components can reach speeds of several kilometers per second and excite seismic waves (Hasselmann, 1963). This is most easily understood for a sinusoidal ocean wave train

over a sinusoidal bottom topography. The main difference between our treatment and the one by Fukao et al. (2010) and Saito (2010) is that we will consider the modulation of the ocean wave amplitude and wavelength at the scale of the bottom topography. We shall see that this modulation is irrelevant for the lowest-order horizontal force, but it dominates the vertical force. Indeed, the magnitude of the two forces is controlled by two different small parameters that are the bottom slope for the horizontal force and a modulation index for the vertical force. Their ratio is a parameter α that is only a function of the product of the mean ocean wave wavenumber k_0 with the mean water depth D_0.

2.1. Sinusoidal Bottom

We consider a varying water depth $\mathrm{D}(x)$ with a mean depth D_0 and amplitude d_0, given by

$$\mathrm{D}(x) = \mathrm{D}_0 - \mathrm{d}(x) = D_0 - \mathrm{d}_0 \cos(k_b x). \tag{1}$$

A monochromatic wave train of radian frequency $\sigma = 2\pi f$ and amplitude a propagating in the x direction has a surface elevation

$$\zeta(x,t) = va(x)\cos\left[S(x) - \sigma t\right] \tag{2}$$

with the phase

$$S(x) = \int_0^x k(x')\mathrm{d}x'. \tag{3}$$

The local wavenumber $k(x)$ oscillates around k_0, adjusting to the depth $\mathrm{D}(x)$ via the dispersion relation (e.g., Mei, 1989),

$$\sigma^2 = gk(x)\tanh\left[k(x)\mathrm{D}(x)\right]. \tag{4}$$

Following Hasselmann (1963), the local amplitude $a(x)$ oscillates around a_0 to keep a constant energy flux while the depth $D(x)$ and group speed $C_g(x)$ vary around D_0 and C_{g0}. From linear wave theory the energy flux is proportional to

$$C_g(x)a^2(x) = C_{g0}a_0^2, \tag{5}$$

with

$$C_g = \sigma/k[0.5 + k\mathrm{D}/\sinh(2k\mathrm{D})]. \tag{6}$$

This conservation of the energy flux is not exact and is perturbed by bottom friction and wave scattering, causing changes in wave height up to 50% over a distance of 40 km (Ardhuin et al., 2003; Roland & Ardhuin, 2014; WISE Group, 2007), while the transfer of ocean wave energy to seismic energy is negligible, typically less than 0.1% over 1000 km. Processes that cause small changes in wave height over one seismic wavelength do not modify the generation of seismic waves (supporting information Figure S1). Only depth-induced breaking can produce a strong local variation of the wave heights that strongly modify the spectrum of the bottom pressure and the seismic response (Ardhuin et al., 2015; Hasselmann, 1963).

We thus transform $a(x)$ given by energy conservation into bottom pressure using linear theory (e.g., Mei, 1989), with ρ_w the density of seawater that is assumed constant,

$$p(z = -\mathrm{D}) = \frac{\rho_w g}{\cosh(k(x)\mathrm{D}(x))}a(x)\cos\left[S(x) - \sigma t\right]. \tag{7}$$

Neglecting bottom friction, which is discussed in section 4, the horizontal force per unit area on the bottom is the bottom pressure times the bottom slope $d'(x)$,

$$\tau(z = -\mathrm{D}) = -\frac{\rho_w g}{\cosh(k(x)\mathrm{D}(x))}a(x)\mathrm{d}_0 k_b \sin(k_b x)\cos\left[S(x) - \sigma t\right]. \tag{8}$$

Here we focus on the components of $p(z = -\mathrm{D})$ and $\tau(z = -\mathrm{D})$ at wavelengths much longer than $2\pi/k_0$. In the case of the horizontal force, the product of slope and pressure partially aliases the wave pattern into shorter $k + k_b$ and longer $k - k_b$ components.

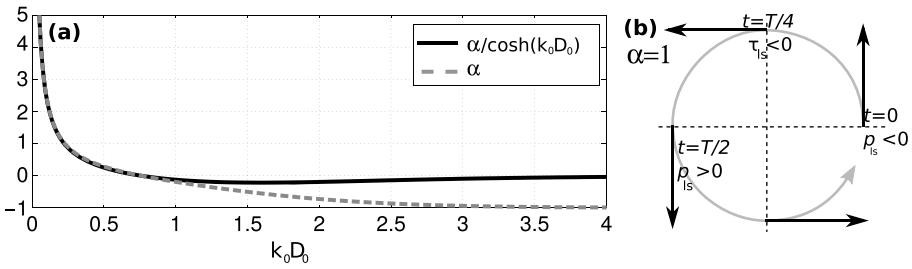

Figure 2. (a) Modulation factor α for the large-scale bottom pressure amplitude, as a function of the nondimensional mean water depth k_0D_0, as given by equation (12). (b) Phases of τ_{ls} and p_{ls} for $\alpha = 1$ at $x = 0$, giving forces (black arrows) with a positive work in the case of retrograde motion with $k_0 - k_b > 0$ (gray arrow), corresponding to Rayleigh waves propagating to the right.

Here it is useful to introduce the nondimensional modulation index

$$\epsilon = -\frac{\mathrm{d}_0}{k_b}\frac{\partial k_0}{\partial \mathrm{D}_0}. \tag{9}$$

In the supporting information (see also Ardhuin & Herbers, 2002; Cuyt et al., 2008), we demonstrate that the modulated cosine gives a Fourier decomposition $\cos[S(x) - \sigma t] \simeq \cos(k_0 x - \sigma t) + O(\epsilon)$. We can thus approximate

$$\begin{aligned} -\sin(k_b x)\cos\left[S(x) - \sigma t\right] &= -\sin(k_b x)\cos(k_0 x - \sigma t) + O(\epsilon) \\ &\simeq \frac{1}{2}\left\{\sin[(k_0 - k_b)x - \sigma t] - \sin[(k_0 + k_b)x - \sigma t]\right\}. \end{aligned} \tag{10}$$

The first term has a wavenumber $K = k_0 - k_b$ which is very small for $k_b \simeq k$. In other words, the horizontal force contains very large wavelengths when the bottom topography and surface waves have nearly equal wavelengths. This large-scale (ls) component of the horizontal force is proportional to the amplitude d_0 of the bottom oscillations,

$$\tau_{ls} \simeq \frac{\rho_w g k_0}{\cosh(k_0 \mathrm{D}_0)}\frac{a_0 \mathrm{d}_0}{2}\sin\left[(k_0 - k_b)x - \sigma t\right]. \tag{11}$$

This expression is valid to order ϵ^0. Modulation effects only come in at order ϵ, with a small correction to the horizontal force.

The large-scale vertical force is more complex. In their analysis, Fukao et al. (2010) neglected the variations in the wave amplitude and phase function. Using $k(x) = k_0$, $a(x) = a_0$, and $S(x) = k_0 x$, they concluded that the *topographic coupling mechanism generates only horizontal force but not vertical force*. In other words, they assumed sinusoidal ocean waves propagating over a flat bottom, which only produces a local bottom deformation known as compliance, which is not a seismic wave (Crawford et al., 1991). In reality, the waves are modified by two modulation effects. First, the phase function $S(x)$ is not exactly periodic and contains a modulated wave number $k(x)$. Second, the bottom pressure amplitude combines the effect of a varying transfer function $G_p(x) = 1/\cosh(kD(x))$ that transforms surface elevation into bottom pressure and a modulation of wave amplitude $a(x)$ associated with the conservation of energy flux. Hence, the horizontal and vertical forces are caused by two completely different effects. For the horizontal force, the bottom slope directly introduces a modulation of the surface waves by the scales of the bottom topography. In the case of the vertical force, the modulation comes from a modification, at the scale of the bottom topography, of the amplitude and wavelength of the wave-induced bottom pressure amplitude. The supporting information provides a derivation of the ratio α of the large-scale vertical force, which excites Rayleigh waves, and the large-scale horizontal force that excites both Rayleigh and Love waves. It is only a function of $y = k_0 D_0$, plotted in Figure 2a,

$$\alpha(y) = \frac{y - \cosh(y)\sinh^3(y)}{\left[y + \sinh(y)\cosh(y)\right]^2}. \tag{12}$$

In the limit of small bottom amplitudes, that is, $\epsilon \ll 1$, the large-scale pressure is

$$p_{ls} = -\alpha \frac{\rho_w g k_0}{\cosh(k_0 D_0)} \frac{a_0 d_0}{2} \cos\left[(k_0 - k_b)x - \sigma t\right]. \tag{13}$$

In the numerator of equation (12) the wavenumber modulation gives $y + \sinh(y)\cosh(y)$ which dominates in shallow water, and the pressure amplitude modulation gives $-[\sinh(y)\cosh(y) + \cosh(y)\sinh^3(y)]$ that dominates in deeper water. The two exactly cancel for $y = k_0 D_0 \simeq 0.76$, which was determined numerically by Ardhuin et al. (2015). For example, at the frequency $f = 0.064$ Hz, the depth where the change in wavelength compensates the change in pressure amplitude is $D_0 = 30$ m. For $kD > 0.23$, $|\alpha| < 1$ and the horizontal force is larger than the vertical force. This can explain the higher amplitudes of Love waves compared to Rayleigh waves that are often observed for primary microseisms (Juretzek and Hadziioannou, 2016, 2017).

We also note that $k_0 D_0 < 0.76$ corresponds to $\alpha > 0$, in which case the pressure maximum has an opposite phase compared to the case $k_0 D_0 > 0.76$ of Figure 1. For waves propagating toward the shore and $k_0 D_0 < 0.76$, the maximum pressure leads the maximum shoreward force by one quarter period (Figure 2b). This rotation of the large-scale force matches the phase of ground velocities in shoreward propagating Rayleigh waves and is opposite to the phase of seaward propagating Rayleigh waves. As a result, the work of the force transfers more energy to shoreward-propagating Rayleigh waves.

2.2. Random Waves and Random Bottom

Following Hasselmann (1963), the solution is expressed as Fourier-Stieltjes integrals with modal surface elevations amplitudes $dZ_s(\mathbf{k})$ corresponding to the waves of wavenumber vector $\mathbf{k}$, with a norm $k = |\mathbf{k}|$, propagating in the direction of the vector $s\mathbf{k}$ where $s = 1$ or $s = -1$ is a sign index. We now generalize the surface elevation to a superposition of linear waves,

$$\zeta = \sum_s \int\int dZ_s(\mathbf{k}) e^{i(\mathbf{k}\cdot\mathbf{x} - s\sigma t)}, \tag{14}$$

where $\mathbf{x} = (x, y)$ is the horizontal position vector, and k and σ are related by equation (4). Without loss of generality, the bottom elevation is $z = -D + d(\mathbf{x})$ with modal amplitudes $dG(\mathbf{k}_b)$,

$$d = \int\int dG(\mathbf{k}_b) e^{i\mathbf{k}_b\cdot\mathbf{x}}. \tag{15}$$

Only interactions with $\mathbf{K} = \mathbf{k} + \mathbf{k}_b$ such that $|\mathbf{K}| \ll |\mathbf{k}|$ can produce seismic waves (Hasselmann, 1963). As a result, the relevant waves and bottom topography are nearly aligned and refraction can be neglected. This reduces the problem to the previous case of sinusoidal ocean waves over sinusoidal bottoms.

Defining θ_b as the direction of the vector $\mathbf{k}_b$, the force in the x direction is

$$\tau_{ls,x} = \sum_s \int\int\int\int \frac{-\rho_w g i k_b \cos\theta_b}{\cosh(k_0 D)} dZ_s(\mathbf{k}) dG(\mathbf{k}_b) e^{i[(\mathbf{k}-\mathbf{k}_b)\cdot\mathbf{x} - s\sigma t]}, \tag{16}$$

corresponding to equation (8) in Saito (2010).

The power spectral densities of the two components of the horizontal force thus, when defined from positive frequencies only,

$$(F_{T,x}, F_{T,y})(\mathbf{K} = 0, f) = \int\int\int\int \left[\frac{\rho_w g k}{\cosh(kD)}\right]^2 (\cos^2\theta_b, \sin^2\theta_b) \\ E(\mathbf{k}) F_B(\mathbf{k}_b) \delta(f - f(\mathbf{k})) \delta(\mathbf{k} + \mathbf{k}_b - \mathbf{K}) d\mathbf{k} d\mathbf{k}_b \tag{17}$$

with $f = \sigma/(2\pi)$ related to $k = |\mathbf{k}|$ by equation (4). Changing variables in spectral space, $E(\mathbf{k})d\mathbf{k} = E(f, \theta)df d\theta$ where θ is the direction and wave propagation. This allows to remove the delta functions and collapse the four-dimensional integral to one dimension only, in which $\mathbf{k}_b = \mathbf{k}$ and the magnitude of $\mathbf{k}$ is selected by the seismic frequency f,

$$(F_{T,x}, F_{T,y})(\mathbf{K} = 0, f) = \int_0^{2\pi} \left[\frac{\rho_w g k}{\cosh(kD)}\right]^2 (\cos^2\theta, \sin^2\theta) E(f, \theta) F_B(\mathbf{k}) d\theta, \tag{18}$$

where $F_B(\mathbf{k})$ is the double-sided bottom elevation spectrum already used in (equation (2.15) and (2.16); Ardhuin & Magne, 2007).

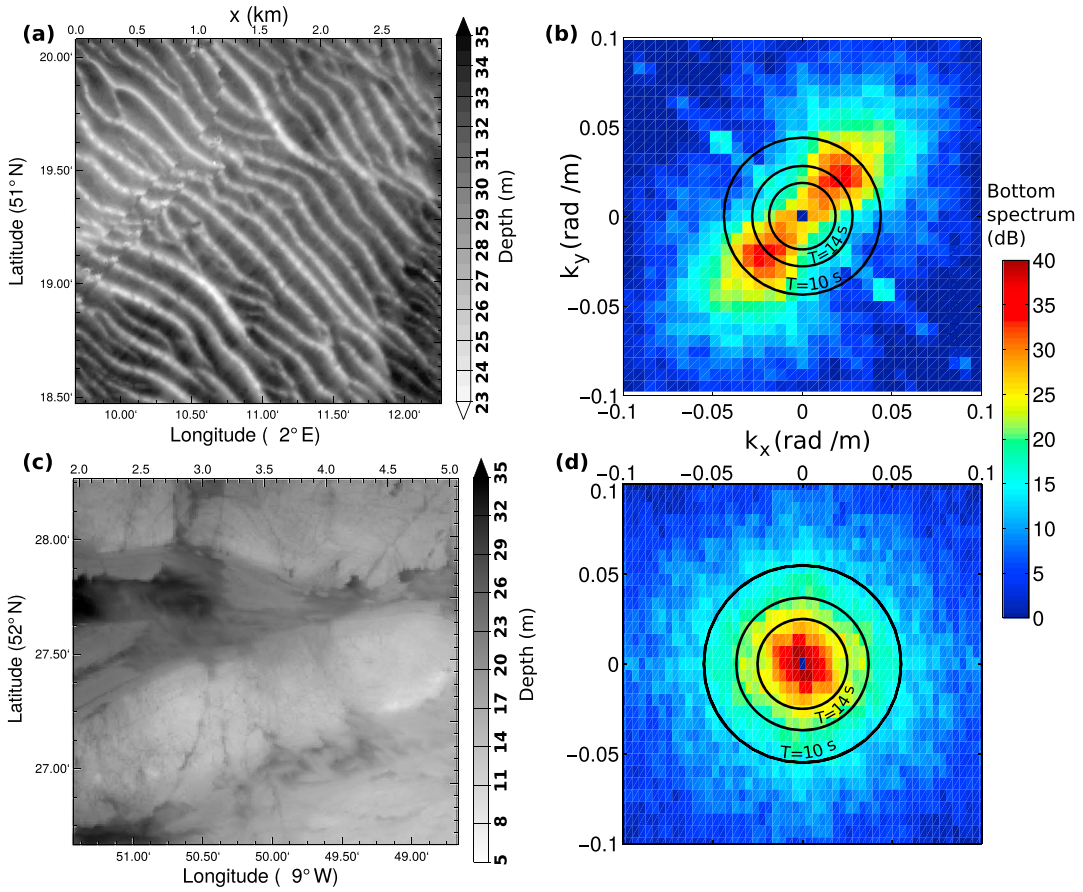

Figure 3. Example of (a) a sandwave field in the southern North Sea and (b) the associated spectrum of the bottom elevation. The circles correspond to the wavenumbers of surface gravity waves with periods 10, 14, and 20 s in $D_0 = 29$-m depth. (c, d) Same format for a rocky platform off the west coast of Ireland between counties Clare and Kerry, with circles corresponding to $D_0 = 15$ m.

For the bottom pressure we define the spectral density F_{p1}. Here the subscript 1 clarifies that this pressure field is different from F_{p2} given by the secondary microseism mechanism due to waves in opposite directions (Ardhuin & Herbers, 2013). The full pressure spectrum is the sum $F_{p1} + F_{p2}$, where we have neglected additional terms from higher-order interactions such as the interactions of two surface waves and one bottom component giving $\mathbf{K} = \mathbf{k} + \mathbf{k}' + \mathbf{k}_b$. That type of interaction is beyond the scope of the present paper.

With the same method that gave the horizontal force (18), we now obtain the pressure power spectral density

$$F_{p1}(\mathbf{K}=0,f) = \int_0^{2\pi} \left[\frac{\rho_w g k \alpha}{\cosh(kD)}\right]^2 E(f,\theta) F_B(\mathbf{k}) \mathrm{d}\theta. \tag{19}$$

For most purposes, these distributed forces over an area dA and in the frequency band df can be replaced by an equivalent oscillating point force (e.g., Gualtieri et al., 2013, equation (2) with an r.m.s. amplitude given here for the vertical force

$$F_{f,\mathrm{d}A,\mathrm{d}f,z}(\mathbf{K}=0,f) = 2\pi\sqrt{F_{p1}(\mathbf{K}=0,f)\mathrm{d}A\mathrm{d}f}. \tag{20}$$

2.3. Magnitude of the Vertical Force Compared to That Over a Slope

To obtain an order of magnitude of this interaction, we use the bottom spectrum of North Sea sandwaves shown in Ardhuin and Magne(2007, Figure 7) and reproduced here in Figures 3a and 3b. This bottom has a maximum power spectral density $F_{B,\max} \simeq 2,400$ m^4 for $k_b = 0.02$ rad/m. Such sandwaves are generated by tidal currents (Besio et al., 2006; Hino, 1968). More typical values of $F_{B,\max}$ are 2 orders of magnitude lower for

sand or silt regions where sandwaves are absent, but they can also be large over rocky seafloors, as shown in Figures 3c and 3d.

We consider a 100-km^2 rocky platform with water depths around $D_0 = 15$ m and ocean waves with 14 s period, with a surface elevation variance of 1 m^2 in deep water, corresponding to a significant wave height of 4 m. Neglecting dissipative processes, wave shoaling from depth D_A (in deep water) to D_0 will cause a change of wavenumber from k_A to k_0, group speed from C_{gA} to C_{g0}. The surface elevation variance is amplified by a factor $k_0 C_{gA}/k_A C_{g0} \simeq 2$ (e.g.,O'Reilly & Guza, 1993). We take a bottom elevation spectral density $F_B(\mathbf{k}_b) = 150$ m^4, consistent with Figures 3c and 3d. Using equation (20), this rocky seafloor gives a force amplitude $N_1 = 2.1 \times 10^9$ N.

We now estimate the force amplitude over a bottom with a constant slope β considered by Hasselmann (1963) and Ardhuin et al. (2015) that is uniform over $L_y = 100$ km in the alongshore direction. The bottom pressure spectral density is

$$F_{p1,\mathrm{slope}}(\mathbf{K}=0,f) = \beta \frac{\rho_w^2 g^4 \left[E_A(f,\theta_n) + E_A(f,\theta_n+\pi)\right]}{k_A (2\pi f)^4 32 L_x} \tag{21}$$

where $E_A(f,\theta_n)$ is the spectral density frequency-direction spectrum of wave energy at the reference depth D_A and in the shore-normal direction θ_n and L_x is the cross-shore distance over which the source is distributed. We consider the same wave spectrum with a narrow Gaussian directional distribution of half-width $\sigma_\theta = 10°$,aaround the shore-normal direction, and a narrow frequency spectrum around 0.07 Hz. This gives a maximum spectral density $E_A(f,\theta) = E_A(f)/(\sigma_\theta\sqrt{2\pi}) \simeq 2.3 E_A(f)$. The area of sources is $\mathrm{d}A = L_x L_y$, giving a r.m.s. vertical force amplitude $N_{1,\mathrm{slope}} = 1.8 \times 10^8$ N that is 10 times smaller than N_1. Besides, $N_{1,\mathrm{slope}}$ goes to zero for other wave directions whereas N_1 is independent of the surface wave direction.

We thus conclude that a realistic wavy bottom can be a more powerful source of primary microseisms than a bottom with a constant slope. The relative importance of the two types of topographies is probably specific to the location considered, with possible hot spots of microseism generation where the bottom is *rough*. Rough here means that topography with wavelengths mathching those of surface waves has a large amplitude. A practical evaluation of this effect for a period of 14 s requires maps of water depths at resolutions of 50 m or better. Unfortunately, such data are not yet available everywhere. For example, the coarser 220-m resolution data provided by the EMODnet project (http://portal.emodnet-bathymetry.eu/) suggest that rough rocky topographies can be found in regions off the outer Hebrides, and at many places along the Norwegian coast, while sandwaves are a prevalent feature of the southern North Sea.

3. Application With a Real Bottom Topography

The bottom pressure spectrum can be transformed into seismic wave amplitudes using Green's function for the equivalent point force (e.g., Gualtieri et al., 2013) or a radiative balance on the seismic energy following Hasselmann (1963). Here we use the latter approach and consider only the response to the vertical force, using the most simple seismic propagation model of a water layer over a half space. This crude model misses the possible effects of sediment layers that can damp or amplify the seismic sources (Gualtieri et al., 2014; Ying et al., 2010). The spectral density of the vertical ground displacement $F_\delta(f)$ at a seismic station is the sum of seismic sources along great circles around the Earth.

Combining equations (S1) and (S2) of Ardhuin et al. (2015) gives

$$F_\delta(f) = 4\pi^2 f \frac{c^2}{\beta_s^5 \rho_s^2} \int F_{p1}(K=0,f) P \frac{\exp(-2\pi f \Delta R_E/UQ)}{R_E \sin\Delta} \mathrm{d}A, \tag{22}$$

where $\mathrm{d}A$ is an elementary area of the ocean, U is the seismic group velocity, R_E is Earth's radius, and Δ is the angle at the Earth center between source and seismic station. c is a nondimensional seismic source coefficient (Gualtieri et al., 2014; Longuet-Higgins, 1950), ρ_s is the crust density, and β_s is the shear wave speed in the crust. Here we use $c = 0.2$, $\rho_s = 2,600$ kg/m^3, $\beta_s = 2,800$ km/s, and $UQ = 720$ km/s. We further set $P = 1$, which is a poorly known coefficient accounting for three-dimensional seismic propagation effects (Hasselmann, 1963; Szelwis, 1982). Given that we investigate frequencies f around 0.1 Hz, the attenuation factor $b = \exp(-2\pi f X/UQ)$ over the distance X is less than 3×10^{-8} for $X > 20,000$ km, so that we can neglect the propagation of seismic waves over multiple orbits round the Earth.

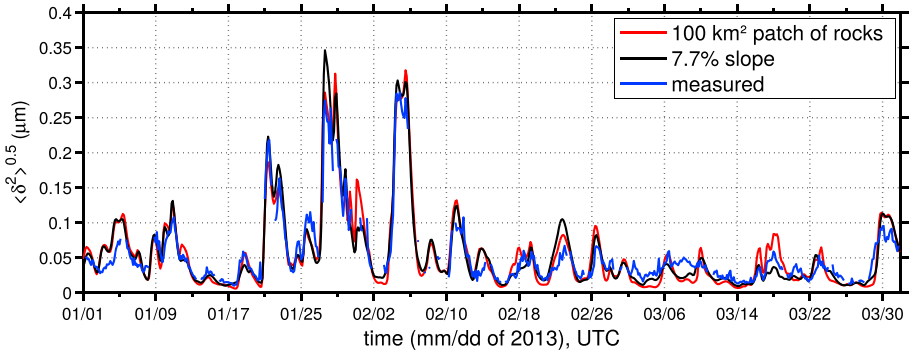

Figure 4. Modeled and measured root mean square vertical ground displacement in the frequency band 0.05–0.073 Hz, at the Glengowla (IGLA) seismometer located in Ireland, 30 km northwest of Galway. The model uses either a the bottom spectrum of Figure 3d, using equation (19) for a 10 by 10 km^2 region located 150 km from the seismic station or source all along the world's shorelines due to a constant slope $\beta = 0.077$ represented by equation (21).

Our estimations of F_{p1} are performed for a single location off the west coast of Ireland, using the numerical wave model output of Rascle and Ardhuin (2013), which is forced by winds from the European Center for Medium range Weather Forecasting operational analyses. We assume that all sources come from a patch of rocky bottom with a spectrum shown in Figure 3d and an area of 100 km^2. That area was adjusted to reproduce the observed seismic amplitude, as shown in Figure 4. The temporal variability of the model and observations shows that storm waves arriving at the Irish coast explain most of the recorded seismic signal. A similar pattern is produced by an effective slope of 7.7% all along the coasts. Given that sources along a constant slope are dominated by the region in water depths D such that $kD \simeq 0.76$ (Ardhuin et al., 2015), this slope should be between 20 and 50 m. The first scenario, with an area of 100 km^2, probably distributed in several patches, is more likely than large-scale slopes exceeding 5% on the continental shelf.

4. Discussion and Conclusions

Whereas Hasselmann (1963) only considered vertical forces and Fukao et al. (2010) only considered horizontal forces, here we have shown that ocean waves propagating over bottom topography of similar wavelengths produce both horizontal and vertical forces of comparable magnitude. The general wave-wave scattering theory yields a rate of growth of the seismic waves during their propagation (Hasselmann, 1966) or, equivalently, a collection of equivalent horizontal and vertical point sources from which a seismic response can be computed.

As we focused on pressure effects, we ignored the modulation of bottom shear stress amplitude τ_b due to varying water depths D. For monochromatic waves, we have $\tau_b \simeq \rho_w f_w a^2 [(2\pi)f / \sinh(kD)]^2$. With a friction factor $f_w \simeq 0.01$ (e.g.,Smyth & Hay, 2002), the shear force amplitude is typically weaker than the pressure amplitude. The modulation of this shear, although different from the pressure modulation due to the $ga/\cosh(kD)$ factor replaced by $f_w(2\pi f)^2 a^2 / \sinh^2(kD)$, should lead to a large-scale horizontal force weaker than the horizontal force discussed above.

As noted in section 2, the combination of horizontal and vertical forces should enhance landward propagating Rayleigh waves and also produce Love waves, possibly explaining the source patterns observed by Juretzek and Hadziioannou (2017). In that paper they also found that the azimuthal radiation patterns of Love and Rayleigh waves require a ratio of the horizontal to vertical forces of the order of $1/\alpha = 1.4$ which in the present theory is obtained for a nondimensional water depth $kD = 0.3$, that is, $D = 6$ m for $f = 0.06$ Hz, with higher ratios for deeper water.

For primary microseisms, estimating the magnitude of the source requires a detailed knowledge of ocean bottom topography at a resolution of 50 m or better. Using examples of real ocean topographies, the vertical force can be much larger over a wavy bottom than over a constant slope. For example, a 100 km^2 source area can explain microseism amplitudes, with frequencies in the range 0.05 to 0.073 Hz, observed at a seismometer in the west of Ireland. A similar magnitude with a constantly sloping bottom requires a 7% slope all along the coast that is not realistic. The dependence of the primary microseism amplitude on the small-scale topography of shelf seas should cause a spatial distribution of sources that could be much more patchy than previoulsy envisaged.

Acknowledgments
Support for this work comes from Agence Nationale de la Recherche, via grant ANR-14-CE01-0012 *MIMOSA*, Labex Mer via grant ANR-10-LABX-19-01, and the National Science Foundation under grant NSF PHY-1748958. I thank Carina Juretzek for the discussions that led to this work, made possible by the support of the COST action ES1401 *Time Dependent Seismology*. Seismic data from the Irish National Seismic Network (INSN) are gratefully acknowledged and can be accessed from http://ds.iris.edu/mda/EI/IGLA. Bathymetry data were provided by the French Service Hydrographique et Oceanographique de la Marine (SHOM; see http://data.shom.fr, in particular https://bit.ly/2KlhhOx), and the Integrated Mapping For the Sustainable Development of Ireland's Marine Resources (INFOMAR) programme and is available at https://maps.marine.ie/infomarbathymetry/. Comments and suggestions from four anonymous reviewers, Victor Tsai and Jeroen Ritsema helped to correct and clarify the manuscript.

References

Ardhuin, F., Balanche, A., Stutzmann, E., & Obrebski, M. (2012). From seismic noise to ocean wave parameters: General methods and validation. *Journal of Geophysical Research*, *117*, C05002. https://doi.org/10.1029/2011JC007449

Ardhuin, F., Gualtieri, L., & Stutzmann, E. (2015). How ocean waves rock the Earth: Two mechanisms explain seismic noise with periods 3 to 300 s. *Geophysical Research Letters*, *42*, 765–772. https://doi.org/10.1002/2014GL062782

Ardhuin, F., & Herbers, T. H. C. (2002). Bragg scattering of random surface gravity waves by irregular sea bed topography. *Journal of Fluid Mechanics*, *451*, 1–33.

Ardhuin, F., & Herbers, T. H. C. (2013). Noise generation in the solid Earth, oceans and atmosphere, from nonlinear interacting surface gravity waves in finite depth. *Journal of Fluid Mechanics*, *716*, 316–348.

Ardhuin, F., Herbers, T. H. C., Jessen, P. F., & O'Reilly, W. C. (2003). Swell transformation across the continental shelf. Part II: Validation of a spectral energy balance equation. *Journal of Physical Oceanography*, *33*, 1940–1953.

Ardhuin, F., & Magne, R. (2007). Scattering of surface gravity waves by bottom topography with a current. *Journal of Fluid Mechanics*, *576*, 235–264.

Besio, G., Blondeaux, P., & Vittori, G. (2006). On the formation of sand waves and sand banks. *Journal of Fluid Mechanics*, *557*, 1–27.

Crawford, W. C., Webb, S. C., & Hildebrand, J. A. (1991). Seafloor compliance observed by long-period pressure and displacement measurements. *Journal of Geophysical Research*, *103*(B5), 9895–9916.

Cuyt, A., Petersen, V., Verdonk, B., Waadeland, H., & Jones, W. B. (2008). *Handbook of Continued Fractions for Special Functions*. Cambridge: Springer.

Friedrich, A., Krager, F., & Klinge, K. (1998). Ocean-generated microseismic noise located with the Grafenberg array. *Journal of Seismology*, *2*, 47–64.

Fukao, Y., Nishida, K., & Kobayashi, N. (2010). Seafloor topography, ocean infragravity waves, and background Love and Rayleigh waves. *Journal of Geophysical Research*, *115*(10), B04302. https://doi.org/10.1029/2009JB006678

Gualtieri, L., Stutzmann, E., Capdeville, Y., Ardhuin, F., Schimmel, M., Mangeney, A., & Morelli, A. (2013). Modelling secondary microseismic noise by normal mode summation. *Geophysical Journal International*, *193*, 1732–1745. https://doi.org/10.1093/gji/ggt090

Gualtieri, L., Stutzmann, E., Farra, V., Capdeville, Y., Schimmel, M., Ardhuin, F., & Morelli, A. (2014). Modelling the ocean site effect on seismic noise body waves. *Geophysical Journal International*, *193*, 1096–1106. https://doi.org/10.1093/gji/ggu042

Hasselmann, K. (1963). A statistical analysis of the generation of microseisms. *Reviews of Geophysics*, *1*(2), 177–210.

Hasselmann, K. (1966). Feynman diagrams and interaction rules of wave-wave scattering processes. *Reviews of Geophysics*, *4*(1), 1–32.

Hino, M. (1968). Equilibrium-range spectra of sand waves formed by flowing water. *Journal of Fluid Mechanics*, *34*, 565–573.

Juretzek, C., & Hadziioannou, C. (2016). Where do ocean microseisms come from? A study of Love-to-Rayleigh wave ratios. *Journal of Geophysical Research*, *121*, 6741–6756. https://doi.org/10.1002/2016JB013017

Juretzek, C., & Hadziioannou, C. (2017). Linking source region and ocean wave parameters with the observed primary microseismic noise. *Geophysical Journal International*, *211*, 1640–1654. https://doi.org/10.1093/gji/ggx388

Longuet-Higgins, M. S. (1950). A theory of the origin of microseisms. *Philosophical Transactions of the Royal Society A*, *243*, 1–35.

Mei, C. C. (1989). *Applied dynamics of ocean surface waves* (2nd ed.). Singapore: World Scientific.

Nishida, K., Kawakatsu, H., Fukao, Y., & Obara, K. (2008). Background Love and Rayleigh waves simultaneously generated at the Pacific ocean floors. *Geophysical Research Letters*, *35*, L16307. https://doi.org/10.1029/2008GL034753

O'Reilly, W. C., & Guza, R. T. (1993). A comparison of two spectral wave models in the Southern California Bight. *Coastal Engineering*, *19*, 263–282.

Rascle, N., & Ardhuin, F. (2013). A global wave parameter database for geophysical applications. Part 2: Model validation with improved source term parameterization. *Ocean Modelling*, *70*, 174–188. https://doi.org/10.1016/j.ocemod.2012.12.001

Retailleau, L., Boué, P., Stehly, L., & Campillo, M. (2017). Locating microseism sources using spurious arrivals in intercontinental noise correlations. *Journal of Geophysical Research*, *122*, 8107–8120. https://doi.org/10.1002/2017JB014593

Roland, A., & Ardhuin, F. (2014). On the developments of spectral wave models: Numerics and parameterizations for the coastal ocean. *Ocean Dynamics*, *64*(6), 833–846. https://doi.org/10.1007/s10236-014-0711-z

Saito, T. (2010). Love-wave excitation due to the interaction between a propagating ocean wave and the sea-bottom topography. *Geophysical Journal International*, *182*, 1515–1523.

Shapiro, N. M., Campillo, M., Stehly, L., & Ritzwoller, M. H. (2005). High-resolution surface-wave tomography from ambient seismic noise. *Science*, *307*, 1615–1617. https:doi.org/10.1111/j.1365-246X.2006.03240.x

Smyth, C., & Hay, A. E. (2002). Wave friction factors in nearshore sands. *Journal of Physical Oceanography*, *32*, 3490–3498.

Szelwis, R. (1982). Modeling of microseismic surface wave source. *Journal of Geophysical Research*, *87*, 6906–6918.

WISE Group (2007). Wave modelling—The state of the art. *Progress in Oceanography*, *75*, 603–674. https://doi.org/10.1016/j.pocean.2007.05.005

Ying, Y., Bean, C. J., & Bromirski, P. D. (2010). Propagation of microseisms from the deep ocean to land. *Geophysical Research Letters*, *41*, 6374–6379. https://doi.org/10.1002/2014GL060979